Space Sci Rev (2017) 206:471–493
DOI 10.1007/s11214-016-0262-3

F-Region Dynamo Simulations at Low and Mid-Latitude

Astrid Maute[1] · **Arthur D. Richmond**[1]

Received: 14 March 2016 / Accepted: 1 June 2016 / Published online: 12 July 2016

Abstract The "*F*-layer dynamo" or "*F*-region dynamo" concept was introduced by Rishbeth (Planet. Space Sci. 19(2):263–267, 1971a; 19(3):357–369, 1971b). *F*-region winds blow the plasma across magnetic field lines setting up transverse drifts and polarization electric fields leading to equatorial downward current during the daytime and upward current at dusk which were confirmed by satellite observations. In the daytime the *F*-region current can close through the highly conducting *E*-region. At night when the *E*-region conductivity is small the *F*-region dynamo generates polarization electric fields and is mainly responsible for the nighttime drift variations. In the evening the *F*-region dynamo is instrumental in generating an enhanced vertical drift, the pre-reversal enhancement. The current due to the *F*-region dynamo is larger at day than at night, but the *F*-region dynamo contributes approximately 10–15 % to the total current at day versus approximately 50 % at night (Rishbeth in J. Atmos. Sol.-Terr. Phys. 43(56):387–392, 1981). The *F*-region dynamo effects strongly depend on the Pedersen conductivity and therefore on the solar cycle. We will review the influence of the *F*-region dynamo on the ionosphere in general and particularly focus on the role it plays in generating ionospheric currents and magnetic perturbations at low-earth orbiting (LEO) satellite altitudes.

Keywords Ionospheric electrodynamics · *F*-region dynamo · Ionospheric current · Magnetic perturbations · Ionospheric drifts · Numerical modeling

1 Introduction

The theory of the atmospheric dynamo was proposed by Stewart (1882) to explain variations of the geomagnetic field that had been determined to have a strong relation to solar activity. He inferred that winds in the rarefied upper atmosphere might generate currents by moving

✉ A. Maute
maute@ucar.edu

A.D. Richmond
richmond@ucar.edu

[1] P.O. Box 3000, Boulder, CO 80307, USA

the conducting gas through the geomagnetic field, a mechanism now called the ionospheric wind dynamo, or simply ionospheric dynamo (e.g., Richmond 1979; Heelis 2004; Fejer 2011).

The ionospheric dynamo effects strongly depend on the ionospheric conductivities. Quantitative modeling of the conductivity (e.g., Hirono 1952; Baker and Martyn 1953) showed it to be highly anisotropic, with very large conductivity parallel to the magnetic field **B**, with Pedersen conductivity enabling current perpendicular to **B** in the direction of the electric field **E**, and with Hall conductivity enabling current perpendicular to both **B** and **E**. The Pedersen and Hall conductivities are largest in the daytime ionospheric E-region, roughly 90–150 km altitude, but there is sufficient Pedersen conductivity in the F-region (approximately 150–500 km) to allow measurable conductive current flow there, as well.

Modeling of winds at F-region heights based on the measured global pattern of thermospheric density (e.g., Geisler 1967) showed that large winds exist there. Rishbeth (1971a,b) pointed out that these F-region winds can have a modest effect on ionospheric electrodynamics at day and a dominant effect at night, when the E-region conductivity is low. He called this effect the "F-layer dynamo" or "F-region dynamo" (Rishbeth 1981, 1997).

Whereas winds in the E-region are strongly influenced by complex upward-propagating atmospheric tidal oscillations, winds in the F-region tend to have a simpler pattern associated with the daily thermospheric pressure variations and with frictional drag caused by ion drag and viscosity. However, the dynamics of F-region winds is complicated by the fact that ion drag is proportional to the electric current density, which in turn is determined largely by the ionospheric wind dynamo. The F-region conductivity is also influenced by ion transport associated with the dynamo electric field. Thus the wind and conductivity are strongly interconnected with the electric field and current, and all these dependencies need to be included in models of the F-region dynamo.

The F-region is strongly coupled to the E-region by the large conductivity parallel to the magnetic field. Parallel electric fields are shorted out, so that the electric field is essentially perpendicular to **B**. On time scales longer than a minute or so the electric field is a potential field, and geomagnetic field lines are equipotential. F-region plasma moves according to the "frozen-in magnetic flux" theorem, with all ions and electrons along a magnetic field line convecting in concert to another field line at the perpendicular velocity $\mathbf{E} \times \mathbf{B}/B^2$. Slight departures from this frozen-in motion occur to account for the existence of the differential ion and electron velocities needed to support electric current perpendicular to **B**.

In the E-region, ion-neutral collisions become sufficiently frequent to prevent ions from moving at the $\mathbf{E} \times \mathbf{B}/B^2$ velocity. To a significant extent, momentum extracted from the neutral wind in the F-region is transferred to air in the E-region on the same magnetic field line, in association with field-aligned electric current, although some of the momentum is also transferred to neighboring field lines. Because the mass of E-region air is much greater than the mass of F-region air, F-region winds are much more strongly affected by the momentum transfer than E-region winds are.

The conductivity is proportional to the plasma density, which has a fairly predictable distribution in the daytime E-region but is much more variable in the F-region and in the nighttime E-region. The conductivity also depends strongly on the magnetic field and on ion-neutral and electron-neutral collision frequencies, which are proportional to the neutral density. The F-region dynamo involves mainly the Pedersen conductivity, which is essentially proportional to the product of the ion density and the neutral density in the F-region, both of which have large solar-cycle variations, as well as variations with local time, season, and geographic location. At Arecibo (18°N, 67°W, $\sim 30°$ magnetic latitude) Burnside et al. (1983) found that the height-integrated nighttime F-region Pedersen conductivity increases about eight times from solar minimum to solar maximum, and at solar maximum

is about ten times as large as the height-integrated nighttime E-region Pedersen conductivity. The F-region dynamo is therefore much more effective at solar maximum than at solar minimum.

During the day the E-region conductivity is large enough to short out most of the electric fields generated by the F-region dynamo (Rishbeth 1971a,b), although at low latitudes the F-region dynamo can be significant even at day (Rishbeth 1971b; Crain et al. 1993a). At night the E-region conductivity becomes much smaller, and the F-region dynamo becomes the dominant driver of plasma convection in the evening low-latitude F-region (e.g., Heelis et al. 1974; Matuura 1974; Farley et al. 1986; Eccles 1998a; Heelis 2004; Rodrigues et al. 2012; Heelis et al. 2012; Richmond et al. 2015; Richmond and Fang 2015). However, even at night the E-region conductivity affects the electric field of the F-region dynamo and the wind at F-region heights (Rishbeth 1971a,b; Evonosky et al. 2016).

The F-region dynamo is responsible for a number of observable effects in the upper atmosphere. Rishbeth (1971b) noted that westward morning winds drive downward F-region current at low magnetic latitudes, while eastward nighttime winds drive upward F-region current there. These currents are associated with a latitude gradient of the zonal magnetic field at low-Earth-orbit (LEO) altitudes. Such magnetic effects were first observed by Maeda et al. (1982) with Magnetic Field Satellite (Magsat) around dusk, where the equatorial current is upward. Maeda et al. (1985) showed that the current intensity varied strongly with solar activity, and Takeda and Maeda (1983) pointed out that the F-region dynamo could explain the observed effects. Closer to mid-day Lühr and Maus (2006) and Lühr et al. (2015) found the effects of downward current at the equator, associated with the westward wind expected at that time. Using 5 years of CHAMP observations Park et al. (2010) quantified the seasonal, solar cycle, diurnal and longitudinal variation of the equatorial vertical current in the F-region.

The zonal currents derived from satellite observations (Shore et al. 2013; Tozzi et al. 2015; Lühr et al. 2016) include effects due to the F-region dynamo and the zonal electric fields, and due to the gravitational and pressure-gradient forces on the plasma, and therefore extracting the F-region dynamo current is challenging. Despite these difficulties Lühr et al. (2016) explained how meridional thermospheric winds directed from the summer hemisphere to the winter hemisphere drive eastward current in the summer hemisphere and westward current in the winter hemisphere, as observed by the Swarm constellation.

The equatorial vertical current connects to the geomagnetic field-aligned current flowing between the F- and E-regions and to the cross-field (meridional and zonal) current in the E-region, with the establishment of a vertical/meridional cross-field polarization electric field that maps between the E- and F-regions and is associated with zonal plasma $E \times B$ drifts in the F-region (Rishbeth 1971b). To the extent that the vertical/meridional current closes on individual field lines at low latitudes, the zonal $E \times B$ drift can be calculated from the average zonal wind on the field line, weighted by the Pedersen conductivity (Rishbeth 1971b; Anderson and Mendillo 1983; Coley et al. 1994; Eccles 1998b; Rodrigues et al. 2012), although Rodrigues et al. (2012) and Richmond and Fang (2015) showed that the eastward ion velocity is somewhat slower than this in the evening.

At night the zonal plasma drift in the equatorial F-region is predominantly eastward (e.g., Fejer 2011; Fejer et al. 2013). Its strength increases with solar activity (Fejer et al. 1991, 2005; Fejer 2011; Coley et al. 2014). On the bottom side of the low-latitude evening F-region westward plasma drifts are observed (Kudeki et al. 1981; Tsunoda et al. 1981; Fejer 1981; Fejer et al. 1985; Aggson et al. 1987; Coley and Heelis 1989; Haerendel et al. 1992; Eccles et al. 1999; Kudeki and Bhattacharyya 1999; Mathew and Nayar 2012; Lee et al. 2015), which can be attributed to westward winds at low altitudes (Kudeki et al. 1981; Anderson and Mendillo 1983; Rodrigues et al. 2012; Richmond et al. 2015).

The F-region dynamo is also responsible for the pre-reversal enhancement (PRE) of the vertical ion drift often observed at the magnetic equator in the early evening (e.g., Woodman 1970; Scherliess and Fejer 1999; Pacheco et al. 2010; Fejer 2011; Madhav Haridas et al. 2015). In addition to seasonal and longitudinal variations, the vertical drift velocity varies with the level of solar activity (e.g., Fejer et al. 1979; Fejer 2011; Stoneback et al. 2011; Madhav Haridas et al. 2015). Numerical models of the ionospheric dynamo that include F-region dynamo effects typically produce a PRE (e.g., Heelis et al. 1974; Farley et al. 1986; Crain et al. 1993b; Eccles 1998a; Eccles et al. 2015). The PRE increases with solar activity (Fesen et al. 2000; Millward et al. 2001; Heelis et al. 2012; Richmond et al. 2015), and simulations are generally consistent with the observed vertical variation of the vertical drift (Fejer et al. 2014).

Possible mechanisms responsible for the PRE have been examined by Farley et al. (1986), Haerendel et al. (1992), Crain et al. (1993b), Eccles (1998a), Heelis et al. (2012), Richmond and Fang (2015), and Eccles et al. (2015). As described by Eccles (1998a), Richmond and Fang (2015), and Eccles et al. (2015), the vertical drift in the PRE is a requirement of plasma flow continuity in a fixed magnetic field, as represented by the curl-free nature of the electric field. Zonally divergent plasma flow on magnetic field lines that pass through the relatively large nighttime F-region conductivity in the Equatorial Ionization Anomaly (EIA) region require vertically convergent flow in the evening, which comes primarily through plasma upflow across lower-altitude field lines. The upward flow velocity increases with the strength of the evening-time F-region zonal winds and conductivity in the EIA region, and decreases with increasing magnitude of nighttime E-region Pedersen and Hall conductivities (Richmond and Fang 2015).

The F-region dynamo also affects the wind in the upper thermosphere. Ion drag on the wind is proportional to the electric current density perpendicular to the magnetic field, and this current is affected by dynamo electric fields. In addition the F-region conductivity depends on the plasma drifts associated with the dynamo electric field. Akasofu and Dewitt (1965) showed how the force on neutral motions associated with electric currents tends to move the neutrals toward the ion motion, thereby reducing the ion-neutral velocity difference and the current density for a given electric field, as if the Pedersen conductivity were reduced. Volland (1976a,b) showed that this type of feedback limits the current density, even if the actual Pedersen conductivity were to become extremely large. Rishbeth (1971a,b) pointed out that the Ampère ($J \times B$) force of the current tends to balance the pressure-gradient force that drives F-region winds, so that the current depends mainly on the pressure gradient, and is insensitive to the value of the Pedersen conductivity. Evonosky et al. (2016) verified that Rishbeth's concept is approximately valid in the EIA evening ionosphere for moderate to high solar activity, though not at the magnetic equator or for solar minimum. Rishbeth (1971a,b) performed simple estimates of the current density and F-region dynamo effects using this concept, while Matuura (1974) and Heelis et al. (1974) carried out global modeling of F-region dynamo effects associated with thermospheric pressure gradients. Fully interactive models of neutral and ion dynamics and electrodynamics have been described by Namgaladze et al. (1988), Richmond et al. (1992), Roble (1994), Millward et al. (2001), Klimenko et al. (2006), Ren et al. (2009), and Jin et al. (2011).

Although some of the current observed in the F-region is associated with the F-region wind dynamo, other F-region currents are associated with gravitational and pressure-gradient forces on the ionospheric plasma (Eccles 2004; Lühr et al. 2003; Maus and Lühr 2006; Huba et al. 2010a,b; Alken et al. 2011; Maute et al. 2012; Richmond and Maute 2014; Alken et al. 2016) or with field-aligned current flowing between the northern and southern hemispheres (Maeda et al. 1985; Olsen 1997; Yamashita et al. 2002; Park et al. 2011; Lühr

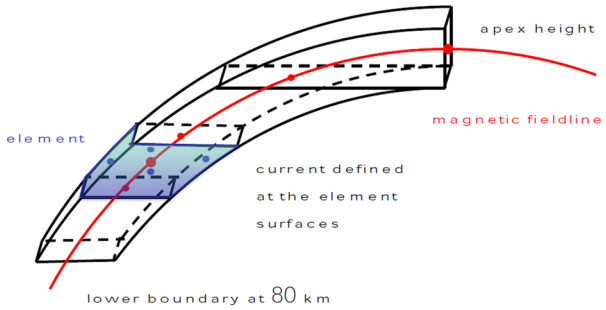

Fig. 1 Schematic of discretization to calculate 3D current

et al. 2015), or between the ionosphere and magnetosphere (e.g., Potemra 1985; Iijima 2000; Weimer 2001; Ohtani et al. 2005; Anderson et al. 2008; Green et al. 2009).

In the remainder of the paper we illustrate the effects of the F-region dynamo and its associated electric field on the ionospheric current and magnetic perturbations using a numerical model. In Sect. 2 we introduce the new numerical model able to calculate the 3-dimensional ionospheric current and its associated magnetic perturbation at the ground and in the ionosphere. This model is used in Sect. 3 to examine the magnitude of the different current sources in Sect. 3.1, the relative magnitude of the E- and F-region dynamo effects in Sect. 3.2, the dependence of the F-region dynamo on the solar cycle in Sect. 3.3, and the impact of non-migrating tides on the current and magnetic perturbation in Sect. 3.4. An example of the total wind driven 3-dimensional current is discussed in Sect. 3.5. In the summary Sect. 4 we reiterate the main points of the F-region dynamo effects on the ionospheric current and magnetic perturbations.

2 Modeling Ionospheric Currents and Magnetic Perturbations

In the following we introduce a new numerical model able to calculate the 3-dimensional ionospheric current system and its associated magnetic perturbations at the ground and in the ionosphere. By considering the height variation of the ionospheric current the magnetic perturbations at low Earth orbit (LEO) satellite height can be more accurately determined compared to the previous approach which assumed that most of the current flows horizontally in an ionospheric sheet current of which the divergence is balanced by field-aligned current (Doumbia et al. 2007; Richmond and Maute 2014).

We briefly describe the structure of the 3-dimensional current model with a representative magnetic flux-tube discretization illustrated in Fig. 1. The model spans altitudes from 80 km to approximately 1000 km and is discretized along magnetic field-lines based on the International Geomagnetic Reference Field (IGRF-12) (Thébault et al. 2015). The vertical grid spacing is defined by fixed-height surfaces which, in the present study, are separated by roughly 1/3 neutral scale height up to 400 km, then by increasingly large increments with increasing height. These height surfaces also define the apex heights of the magnetic field lines used in the discretization. The field-lines intersect the 80 km lower boundary at irregular latitudes, with steps ranging from 0.13° near the magnetic equator to 3.05° at mid-latitudes. The discretization is chosen such that the strong height and latitudinal variations in the low-latitude ionosphere can be resolved. Along the field-line volume elements are introduced with the current determined at the surfaces of each element.

The model is built such that the formulation to solve for the global ionospheric electric potential Φ and ionospheric current $\mathbf{J}$ is consistent and satisfies

$$\nabla \cdot \mathbf{J} = 0 \tag{1}$$

over each element. In Fig. 1 the current is defined at the element surfaces, with the horizontal current transverse to the field line at the blue points and the vertical current at the small red points. The electric potential is solved for at the center of the element (big red point) and the electric field $\mathbf{E}$ can be conveniently calculated from

$$\mathbf{E} = -\nabla \Phi \tag{2}$$

at the blue points through finite differencing of the potentials at the horizontally neighboring large red points. Special considerations are applied at the top equatorial volumes of the flux tubes on either side of the apex. The divergence of the wind driven current $\mathbf{J}_w$ (first two terms on the right hand side of Eq. (3)) and plasma pressure gradient and gravity driven current, $\mathbf{J}_p$ and $\mathbf{J}_g$, respectively, are balanced by the convergence of electric field driven current (first two terms on the left side of Eq. (3)) and field-aligned current $\mathbf{J}_\parallel$ as shown by

$$-\nabla \cdot [\sigma_P \mathbf{E}_\perp + \sigma_H \mathbf{b}_o \times \mathbf{E}_\perp + \mathbf{J}_\parallel] = \nabla \cdot \left[\sigma_P \mathbf{u} \times \mathbf{B}_o + \sigma_H \mathbf{b}_o \times (\mathbf{u} \times \mathbf{B}_o) + \mathbf{J}_p + \mathbf{J}_g\right] \tag{3}$$

with σ_P and σ_H the Pedersen and Hall conductivity, respectively, the neutral wind $\mathbf{u}$, $\mathbf{E}_\perp$ the electric field perpendicular to the geomagnetic main field $\mathbf{B}_o$ with the unit vector $\mathbf{b}_o$. The total magnetic field $\mathbf{B}$ is related to the geomagnetic main field by $\mathbf{B} = \mathbf{B}_o + \Delta\mathbf{B}$ with $\Delta\mathbf{B}$ the magnetic perturbations.

When considering scale sizes of minutes and 100 s of kilometers it is valid to assume that field-lines are equipotential due to the very high conductivity parallel to the field-line (Farley 1959). Using this assumption the 3-dimensional Eq. (3) can be reduced to 2-dimensions by integrating the perpendicular current divergence $\nabla \cdot \mathbf{J}_\perp$ along the magnetic field-line from the bottom of the ionosphere (here 80 km) in one hemisphere to the bottom in the opposite hemisphere (e.g., Richmond 1995; Richmond and Maute 2014). For the present study all field-lines are assumed to connect to the opposite hemisphere, even within the polar cap, so that Φ is hemispherically symmetric. The boundary condition for the field-line integration at the bottom of the ionosphere is the current from the lower atmosphere, which is neglected in this study. The sum of downward field-aligned currents at the top of the model on a field-line is calculated from the empirical models of the high-latitude electric potential (Heelis et al. 1982) and TIE-GCM conductivities. Applying the appropriate equatorial boundary condition that there is no net vertical current the resulting partial differential equation is solved for the electric potential Φ and the electric field is calculated from Eq. (2).

The current perpendicular to the magnetic field-line is calculated by using Eq. (3) leading to the magnetic eastward current density J_{e1} and downward/equatorward current density J_{e2} as defined by (Richmond 1995). The vertical current at a particular height is found by summing up the divergence of the transverse current in the flux-tube elements along a field-line to a particular height taking the boundary conditions into account. The relationship between vertical and field aligned current density is $J_z = -J_\parallel \sin I$ with I being the local inclination of the field-line.

For plotting the currents and for calculating the magnetic perturbations the current densities are mapped to the quasi dipole coordinate system with the magnetic eastward component J_{f1}, the northward component J_{f2}, and the vertical current density J_z (Richmond 1995).

The conductivities, neutral winds and gravity and plasma gradient current, J_g and J_P, are specified by the Thermosphere-Ionosphere-Electrodynamics General Circulation Model

(TIE-GCM). The TIE-GCM is a self consistent numerical model of the thermosphere which includes the dynamics, energetics and chemistry with a self-consistent electrodynamo with the original development by Dickinson et al. (1984), Roble et al. (1988), Richmond et al. (1992) and the interested reader can get more information about the current status in (e.g., Qian et al. 2014; Richmond and Maute 2014, and references therein). The model spans approximately 97 km to 450 to 600 km depending on the solar activity.

Above and below the TIE-GCM boundaries the neutral wind is assigned the boundary values. The conductivities above the TIE-GCM upper boundary, while practically negligible, are assumed to decrease exponentially with the scale height of the neutral atmosphere. Below 97 km the Pedersen and Hall conductivities are assumed to decrease exponentially with scale lengths of 5 km and 3 km, respectively.

The lower thermospheric winds in the TIE-GCM are driven by upward propagating tides, which are global scale waves with periods of a fraction of a solar day (in the present study 24 hrs and 12 hrs) are specified at the lower boundary of the model through the Global Scale Wave Model (GSWM) climatology (Hagan and Forbes 2002, 2003). The tides can either migrate with the apparent motion of the Sun, then they are called migrating tides, or not, and then they are called non-migrating tides. Migrating tides are invariant with longitude and only depend on the local time while non-migrating tidal variations depend on longitude and local time. The GSWM climatology includes migrating and non-migrating tidal specification. In the F-region the neutral wind is mainly forced in-situ by the absorption of solar UV radiation and has a strong migrating diurnal component (e.g., Lindzen 1979).

Alternatively to the TIE-GCM we employ widely used empirical models to specify the neutral wind and conductivities. The Horizontal Wind Model (HWM) (e.g., Hedin et al. 1996) provides the neutral winds, and the ionospheric conductivities are determined using the International Reference Ionospheric (IRI) (e.g., Bilitza et al. 1993) ionospheric parameters and the Mass-Spectrometer-Incoherent-Scatter (MSIS) (e.g., Hedin 1991; Hedin et al. 1996) neutral temperature and densities.

Whereas the ionospheric dynamo component of the TIE-GCM assumes that most of the horizontal current flows in a thin E-region layer and does not calculate the height variation of $J_{\parallel}$ within the ionosphere, our new model treats the ionospheric current as fully three dimensional. We find that the electric potential calculated by the two models is very similar, confirming that the numerical techniques are adequate.

3 F-Region Dynamo Current and Associated Magnetic Perturbations

In observations of ionospheric currents and magnetic perturbations it is very challenging to isolate effects due to certain current sources. Numerical modeling can be used to inform about the general behavior and magnitude of certain current sources under various conditions by studying them in isolation.

In the following we utilize the 3D current model to compare the magnitude of the wind driven current to the gravity and plasma pressure gradient driven current. Gravity and plasma pressure current are reviewed by Alken et al. (2016) in this issue and therefore are not discussed in detail. The focus is on the F-region wind dynamo effects which will be compared to the signals of the E-region wind dynamo reviewed by Yamazaki and Maute (2016) in this issue. The wind field is separated at 150 km into an E-region (F-region) dynamo wind with winds set to zero above (below) 150 km. The separation at 150 km is somewhat arbitrary but should ensure that in the daytime F-region the Pedersen conductivity dominates over the Hall conductivity.

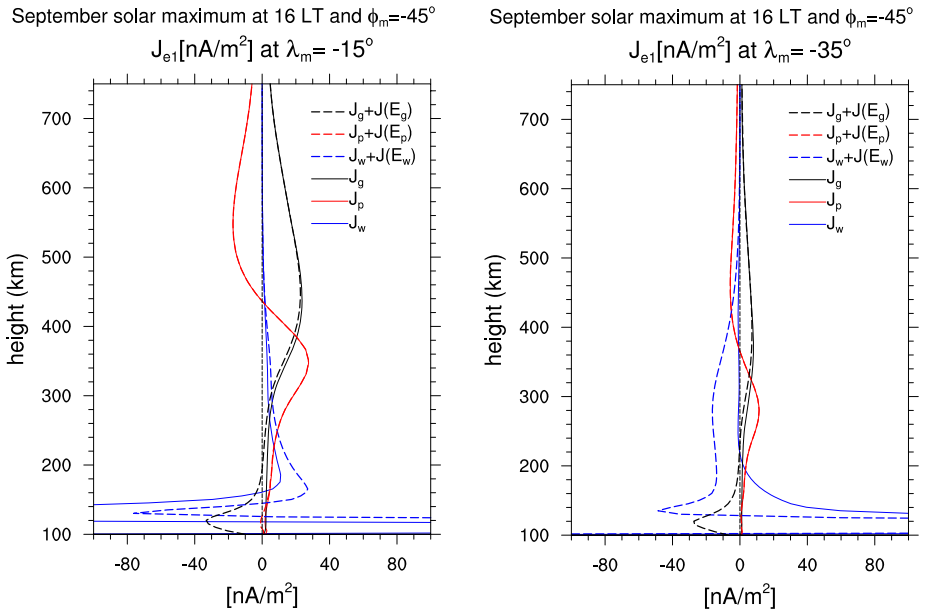

Fig. 2 Magnetic eastard current at approximately 16 local time for September equinox and solar maximum conditions (day of year 264; $F_{10.7} = 200$ sfu; 0 UT; $\phi_m = -45°$ magnetic longitude) due to the neutral wind J_w (*blue line*), gravity J_g (*black line*) and plasma pressure gradient J_p (*red line*) shown by *solid lines*, and due to these forcings and the associated electric field shown by the *dashed lines* at $\lambda_m = -15°$ magnetic latitude (left) and $\lambda_m = -35°$ (right)

3.1 Daytime Current at Low and Mid-Latitude

Figure 2 illustrates the vertical variation of the magnetic eastward current J_{e1} at approximately 16 local time (LT) at $\lambda_m = -15^circ$ and $\lambda_m = -35°$ magnetic latitude for solar maximum conditions during September equinox based on TIE-GCM winds and conductivities. The current due the wind dynamo (blue lines) is compared to the gravity (red lines) and plasma pressure gradient (black lines) driven current. The solid lines illustrates the current represented by the terms within the bracket on the right side of Eq. (3), J_w, J_p and J_g, and the dashed curves represent the total current which includes the effect of the associated electric field, $J(E_w)$, $J(E_p)$ and $J(E_g)$, as represented by the first two terms within the bracket on the left side of Eq. (3).

Figure 2 left depicts the height variation in the equatorial ionization anomaly region (EIA) where the plasma density is high. The EIA is caused by the predominantly eastward low latitude daytime electric field resulting in an upward vertical drift which lifts the plasma at equatorial latitude to higher altitudes till it diffuses down along the magnetic field-lines forming the plasma density enhancements between $|\lambda_m| = 10°$–$20°$ magnetic latitude (Appleton 1954). Gravity and plasma pressure gradient current maximizes in this region with magnitudes of approximately 20 nA/m^2. In the upper F-region these two currents tend to cancel since the plasma pressure force tends to be balanced by the gravitational force. Below the F-region density peak (here around 430 km) the two currents enhance each other with values of up to 40 nA/m^2 and dominate over the wind driven current.

The plasma pressure gradient current J_p tends to close in the F-region and therefore does not set up much of a polarization electric field E_p, as illustrated by the nearly coin-

cident solid and dashed red lines (Alken et al. 2011). The gravity current J_g, however, is mainly eastward and closes through the highly conducting daytime E-region with a westward current generated by a westward electric field E_g (dashed black line). This westward electric field driven current $J(E_g)$ of approximately 30 nA/m^2 is still much smaller than the wind driven current in the E-region (blue lines) which can be over 1000 nA/m^2. The E-region dynamo current is highly variable since it is forced by upward propagating tides from the lower atmosphere and strong due to large Hall conductivity in the E-region.

In the EIA region the wind dynamo generated current $J_w + J(E_w)$ dominates in the lower F-region (up to approximately 250 km) with values of 10–30 nA/m^2. However poleward of the EIA region at $\lambda_m = -35°$ (Fig. 2 right) the plasma density is much lower and the wind driven current $J_w + J(E_w)$ is larger than gravity and plasma pressure gradient current up to 400 km altitude. The wind driven current J_w itself is very small in the F-region (blue solid line) but electric fields E_w are set up, primarily by the E-region dynamo, to ensure current continuity and these generate more significant currents (approximately 20 nA/m^2).

The F-region wind generates an equatorial downward current during the daytime and upward at dusk (e.g., Rishbeth 1971a; Lühr and Maus 2006; Olsen 1997; Lühr et al. 2015). Park and Lühr (2013) estimated the equatorial vertical current J_w and $J(E_w)$ based on CHAMP data. However, in addition to the wind dynamo the gravity and plasma pressure gradient current lead to vertical low latitude currents which are generated by the zonal polarization fields E_g and E_p in the E-region. Vertical currents from all three sources are present at LEO height but with varying magnitudes. At 400 km height under solar maximum conditions the vertical wind dynamo current density reaches values of ± 10 nA/m^2 between $\lambda_m = \pm 10°$ while the gravity and plasma pressure gradient current each attains only ± 1.5 nA/m^2 which is approximately 15 % of the wind driven vertical current. The vertical current caused by the neutral wind dynamo and gravitational force is upward current in the morning and downward at dusk.

3.2 Effects of E- and F-Region Wind Driven Current

In the remainder of the section we consider only the wind dynamo forcing. To compare the effect of E- and F-region dynamos on the ionospheric current and magnetic perturbations numerical experiments were conducted with wind forcing in the E- and F-region (Fig. 3a, b, c), in the F-region only (above 150 km; Fig. 3d, e, f), and in the E-region only (below 150 km; Fig. 3g, h, i). The conductivities are identical for the simulations. In Fig. 3(a, d, g) the height integrated current density J_{f1} and J_{f2} [A/m] is illustrated by vectors and the positive upward vertical current density J_z [A/m^2] at the top of the model (1000 km) by the contours. The conditions are for September equinox and solar maximum ($F_{10.7} = 200$ sfu; 1 sfu $= 10^{-22}$ Wm^{-2} Hz^{-1}). Equinox conditions were chosen in order to minimize the interhemispheric currents.

The total height integrated current (Fig. 3a) has comparable contributions from the F-region (Fig. 3d) and E-region (Fig. 3g), with a clockwise current vortex in the southern hemisphere and an anticlockwise vortex in the northern hemisphere. The narrow band of enhanced eastward current at the magnetic equator is the signal of the equatorial electrojet (EEJ) caused by the combination of the horizontal magnetic field direction, the large ratio of Hall to Pedersen conductivity, and the fact that the atmosphere is assumed to be nonconducting below 80 km (e.g., Forbes 1981; Rastogi 1989).

The F-region dynamo current $J_{wF} + J(E_{wF})$ (Fig. 3d) has a similar vortex pattern as the E-region dynamo current but is weaker (approximately 10–50 % of the total horizontal height integrated current density due to E- and F-region winds between 8–16 LT and

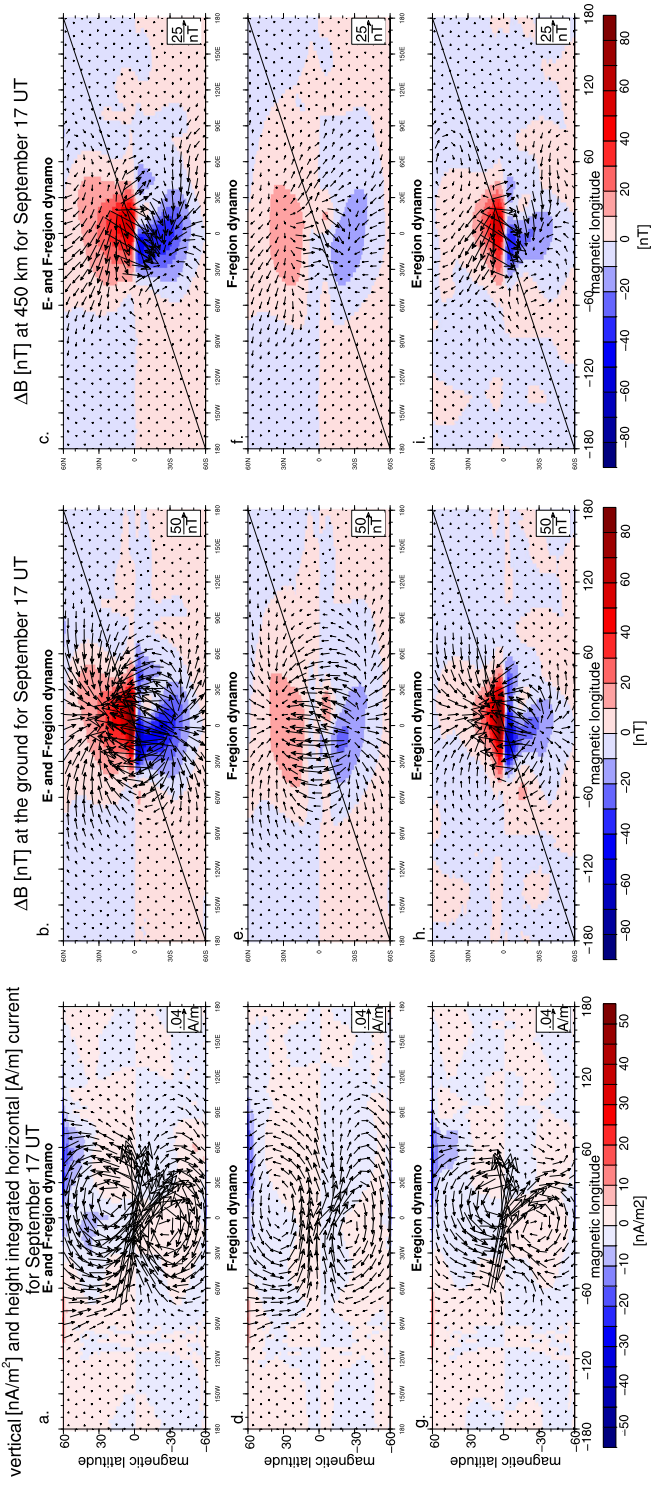

Fig. 3 Left: height integrated horizontal current density (horizontal) and vertical current density (upward positive); Middle: associated magnetic perturbation at the ground; Right: associated magnetic perturbation at 450 km altitude. All plots are over geomagnetic longitude and latitude for September equinox conditions at 17 UT (local noon at approximately 0° magnetic longitude) for solar maximum conditions ($F_{10.7} = 200$ sfu) due to the wind dynamo at all altitudes (top); due to winds above 150 km (middle); due to winds below 150 km (bottom)

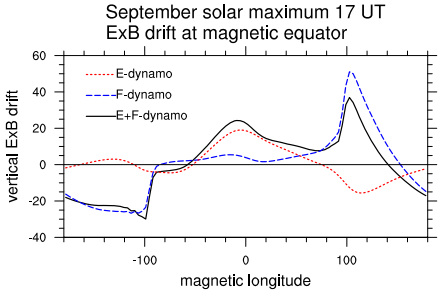

Fig. 4 Longitudinal variation of equatorial upward ExB/B^2 drift for September equinox conditions at 17 UT for solar maximum conditions ($F_{10.7} = 200$ sfu) due to the wind dynamo: wind at all altitudes ($E + F$-dynamo; *black solid line*); wind only above 150 km (F-dynamo, *dashed blue line*); wind only below 150 km (E-dynamo, *red dotted line*)

$|\lambda_m| < 40°$), extends further in longitude/local time (LT) and has slightly different vortex center locations. The F-region dynamo current vortex is mainly caused by the wind in the lower F-region which is less variable than the E-region wind driven by upward propagating tides. In the F-region diurnal solar tides (period of 24 hrs) dominate, which are mainly in-situ forced, and they lead to the F-region vortex longitudinal extent.

Although the E-region dynamo current $J_{wE} + J(E_{wE})$ is in general stronger than the F-region dynamo current $J_{wF} + J(E_{wF})$, at middle latitudes, in the morning and evening, around $\phi_m = \pm 75°$ magnetic longitude in Fig. 3, the height integrated current density due to F-region wind has a comparable magnitude to that of the E-region case. For example in the morning between 6–8 LT the F-region dynamo contributes between 60–80 % to the total height integrated horizontal current density due to E and F-region winds between $|\lambda_m| < 40°$. For the F-region case a broad eastward current between $\lambda_m = \pm 20°$ exists which will be discussed later.

The associated magnetic perturbations at the ground and at 450 km are depicted in the middle and right panels in Fig. 3, respectively, with the arrows showing the horizontal perturbation while the contours represent the upward magnetic perturbation. The reference vector magnitude for the magnetic perturbation at the ground is double that at 450 km. The main signal at the ground for all the cases is the strong vertical and poleward perturbations at low latitudes due to the EEJ. At middle latitude the ground magnetic perturbations tend to have a converging (northern hemisphere) and diverging (southern hemisphere) pattern reflecting the counterclockwise and clockwise current vortex in each hemisphere, respectively. In general the ground magnetic perturbations are stronger than the perturbations at 450 km height, and at middle latitude the direction of the horizontal perturbations is reversed since most of the current is flowing between the ground and LEO altitudes (here 450 km). The magnetic perturbation due to the E- and F-region dynamos can be comparable in size during the daytime at middle latitudes, and around 6 LT and 18 LT.

During the nighttime the current and associated magnetic perturbations due to E- and F-region winds are much smaller because the nighttime conductivities are much smaller than at daytime. Especially the E-region dynamo contribution is at most 30 % of the total nighttime height integrated current density between $|\lambda_m| = \pm 40°$. However, the nighttime equatorial vertical plasma drift is mainly caused by F-region winds, as shown in Fig. 4 for the simulations presented in Fig. 3. While during the daytime the downward F-region current associated with the westward wind is closed easily through the highly conducting E-region (Rishbeth 1971a,b), during the nighttime the E-region conductivity is much smaller. Therefore at night the mainly eastward F-region wind sets up strong polarization fields proportional to the F-region wind. These vertical polarization fields cause an eastward ion drift in the F-region, a westward electric field and a downward ExB drift during most of the night (e.g., Heelis et al. 1974; Farley et al. 1986; Eccles 1998a; Heelis 2004).

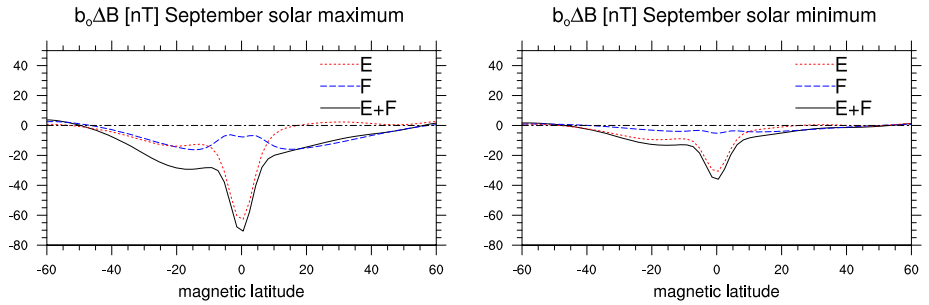

Fig. 5 Scalar magnetic perturbations at 450 km altitude for September equinox conditions at approximately local noon (17 UT) for solar maximum ($F_{10.7} = 200$ sfu) and minimum ($F_{10.7} = 70$ sfu) conditions left and right panel, respectively, due to the wind dynamo: wind at all altitudes ($E + F$-region dynamo; *black solid*); wind only above 150 km (F-region dynamo; *blue dashed*); wind only below 150 km (E-region dynamo; *red dotted*)

Another phenomena of the F-region dynamo is the increase in the equatorial vertical drift in the early evening called the Pre-Reversal Enhancement (PRE) (see Fig. 4 at $\phi_m = 105°$ magnetic longitude) (e.g., Woodman 1970; Fejer et al. 1979; Scherliess and Fejer 1999). Heelis et al. (1974) successfully simulated the PRE by including the F-region dynamo. The strong vertical ion drift is needed for continuity of plasma convection when the F-region conductivity is much larger than the E-region one and the evening eastward wind is increasing toward midnight (Crain et al. 1993b; Eccles 1998a; Richmond and Fang 2015; Eccles et al. 2015).

3.3 Effects of Solar Cycle

From solar activity minimum to maximum the Pedersen conductivity increases comparatively more than the Hall conductivity leading to a more effective F-region dynamo during solar maximum than minimum (e.g., Burnside et al. 1983; Crain et al. 1993a). In Fig. 5 the noon time scalar magnetic field variation at 450 km height for solar maximum ($F_{10.7} = 200$ sfu; left panel) and solar minimum ($F_{10.7} = 70$ sfu; right panel) are compared and separated into the contributions due to E- and F-region neutral wind forcing, depicted by the red and blue lines, respectively. The shown scalar magnetic field $\mathbf{b} \cdot \Delta\mathbf{B}$ describes the magnetic perturbation in the geomagnetic main field direction $\mathbf{b}$. While the latitudinal variation is more or less insensitive to the solar cycle the magnitude is significantly reduced during solar minimum. Analyzing CHAMP observations an almost linear relationship between solar radio flux $F_{10.7}$ and vertical low latitude F-region current was found (Park et al. 2010; Lühr and Maus 2006).

Close to the magnetic equator the equatorial electrojet (EEJ) which is an E-region phenomena is responsible for the magnetic perturbation signal. During solar minimum the E-region wind dynamo is comparatively more important than the F-region wind dynamo. During solar maximum the F-region wind driven current J_{wF} together with the current due to its associated electric field $J(E_{wF})$ can have an equal or larger contribution to the middle and low latitude magnetic perturbation at 450 km compared to the E-region contribution $J_{wE} + J(E_{wE})$ which will be examined in the following.

Figure 6 illustrated the height variation of Hall- and Pedersen-conductivity at approximately 12 LT in the EIA region for solar minimum (red/orange dashed lines) and solar maximum (blue/cyan solid lines). The geophysical conditions, date and time correspond to

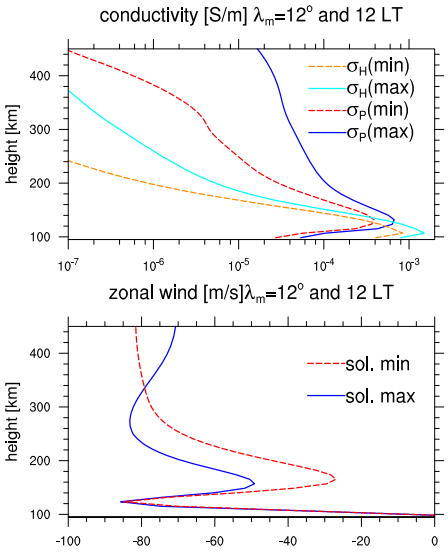

Fig. 6 Noontime Pederson (*blue* and *cyan*) and Hall (*red* and *orange*) conductivity (top panel) and zonal neutral wind (bottom panel) height variation at $\lambda_m = 12°$ (geographic longitude $\phi_g = -75°$, geographic latitude $\lambda_g = 0°$) for September equinox conditions and solar maximum ($F_{10.7} = 200$ sfu, *solid lines*) and minimum ($F_{10.7} = 70$ sfu, *dashed lines*)

the ones in Fig. 5. The F-region Pedersen conductivity increases more strongly with solar cycle than E-region conductivity. Although the absolute Pedersen conductivity is still smaller in the F- than in the E-region the field-line integrated Pedersen conductivity can be larger in the F-region than in the E-region especially for field-lines with apex heights at or above the F-region electron density peak (Crain et al. 1993a).

The F-region neutral wind in Fig. 6 bottom is predominantly in-situ driven by the solar heating while in the E-region upward propagating tides play an important role which is almost independent of the solar cycle. During the daytime the F-region wind at low latitudes is mainly westward.

The westward zonal wind tends to be perpendicular to the main magnetic field and therefore a small ion drift occurs produces a downward current during the daytime (Rishbeth 1971a) illustrated in Fig. 7 top by the simulated downward current density near the equator due to F-region winds. Vertical equatorial currents were derived from Magnetic Field Satellite (Magsat) data by (e.g., Maeda et al. 1982, 1985; Olsen 1997) in the evening and from CHAMP and Swarm observations during the daytime (e.g., Lühr and Maus 2006; Shore et al. 2013; Lühr et al. 2015).

During the daytime the equatorial downward current can easily close meridionally through the E-region as illustrated by the horizontal poleward current density in Fig. 7 top left. An upward/poleward electric field is established as indicated in Fig. 7 bottom panel for the F-region dynamo case under solar maximum and minimum conditions. Since the F-region dynamo forcing is weak during solar minimum the polarization electric field in the E-region is small. The Hall conductivity which peaks around 110 km (Fig. 6) induces an eastward current perpendicular to the upward/poleward electric field and the magnetic field. The eastward current maximizes around 110 km as depicted by the contours in Fig. 7 top panels. The eastward current is much stronger during solar maximum than minimum conditions (Fig. 7), leading to the magnetic perturbations at middle latitudes in the F-region dynamo case (see Fig. 5).

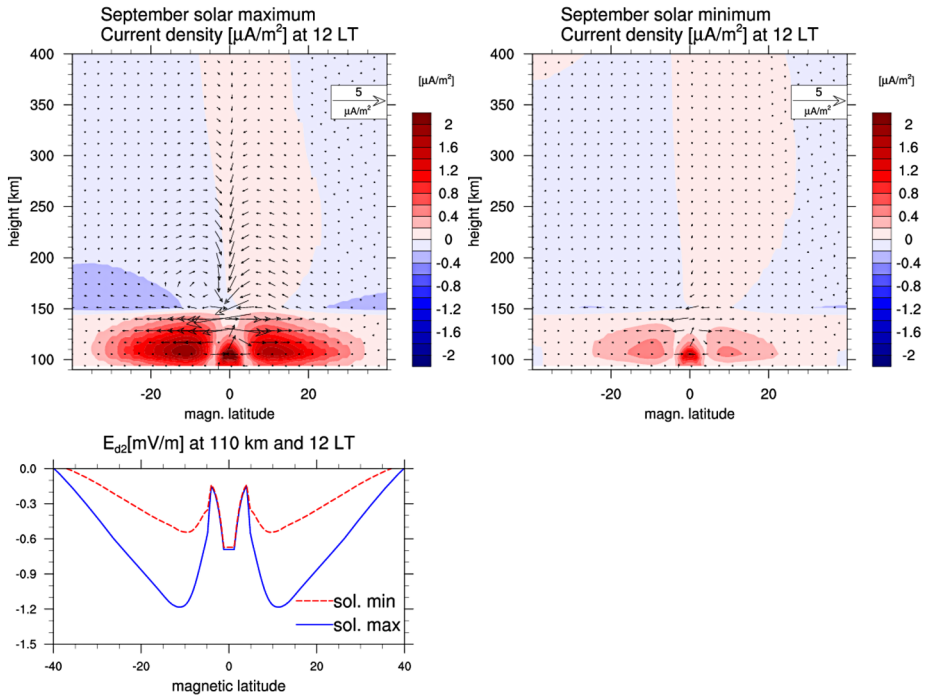

Fig. 7 For the F-region dynamo case (no wind below 150 km): Current density [μA/m^2] at 12 LT (magnetic latitude $\phi_m = -3°$; 17 UT) for September solar maximum (top left panel) and minimum (top right panel). The magnetic eastward horizontal current density (horiz. J_{f1}) is presented by the contours, while the vertical and magnetic northward horizontal current density, J_z and horiz. J_{f2}, respectively, is represented by the vectors. The vertical current density is scaled by the ratio of horizontal to vertical distance of the plot. Downward/equatorward electric field E_{d2} [mV/m] perpendicular to the magnetic field at 110 km and 12 LT for solar maximum and minimum case is shown at the bottom

3.4 Effects of Non-migrating Tides

Although non-migrating tides in general largely dissipate in the E-region, non-migrating tidal winds in the F-region have been derived from satellite observations (e.g., Häusler and Lühr 2009; Häusler et al. 2010; Oberheide et al. 2011; Cho and Shepherd 2015; Xiong et al. 2015). The effect of non-migrating tides was observed in several ionospheric quantities, e.g., plasma distribution (e.g., Immel et al. 2006; Xiong et al. 2014; Pancheva et al. 2012). Park et al. (2010) found a wave number 4 feature in the CHAMP latitudinally integrated sheet current density of the vertical F-region current at low latitudes of 1 mA/m and speculated about the connection to the wave 4 signal found in the cross track winds derived from CHAMP (Häusler and Lühr 2009). In observations one cannot distinguish between the mechanisms of the coupling (e.g., England et al. 2010). Using the model we provide an estimate of the non-migrating tidal effects on F-region current and magnetic perturbations.

To delineate the non-migrating tidal effects we analyze the difference of two TIE-GCM simulations, one with migrating and non-migrating tidal forcing and one with only migrating tidal forcing at the lower boundary. The simulations are for solar minimum conditions $F_{10.7} = 70$ sfu when tides can more freely propagate into the upper atmosphere (e.g., Jones et al. 2013).

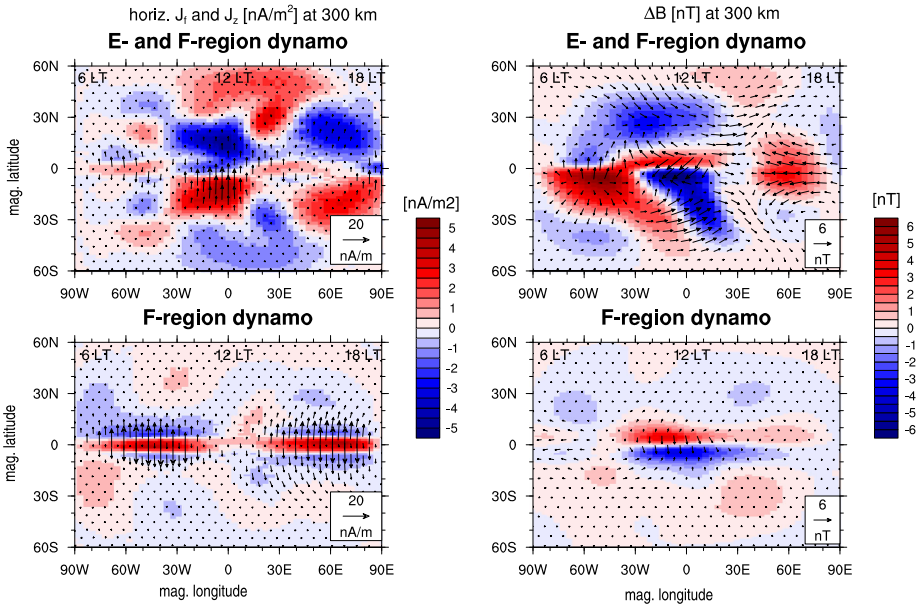

Fig. 8 Daytime variation (6–18 LT) of ionospheric current density [nA/m^2] (left) and magnetic perturbations [nT] (right) at 450 km height due to non-migrating tides for September at 17 UT (local noon approximately at $\phi_m = 0°$ magnetic longitude). Top panels depict variation due to non-migrating tides in the E- and F-region dynamo; bottom panels illustrate variation due to non-migrating tides in the F-region dynamo (wind only above 150 km)

Figure 8 depicts the daytime variations at 300 km due to non-migrating tides between approximately 6 to 18 LT for non-migrating tidal winds in the E- and F-region (top) panels and in the F-region (bottom panels). For non-migrating tides in the F-region the current is confined to low latitude and tends to close in the meridional plane while non-migrating tides in the E-region lead to a more complex current pattern extending to middle latitudes.

Comparing the global average current magnitude at 300 km in Fig. 8 to the one of a simulation with the migrating and non-migrating tidal forcing at the lower boundary can be a rough indicator of the possible relevance of non-migrating tides. The magnitude of the difference current between the full-tide and migrating-only-tide simulations is on average around 25 % of the current which includes migrating and non-migrating forcing (full-tide case). When only F-region non-migrating tides are considered the global-average current magnitude is reduced to 8 % of the current of the full-tide case. This confirms studies that non-migrating tides are more prevalent in the E-region (e.g., Hagan et al. 2009; Oberheide et al. 2011) and suggests that effects due to F-region non-migrating tides are confined to the low latitude current.

The corresponding magnetic perturbations at 300 km (Fig. 8 right panel) reflect the latitudinal extent of the current (left panel). On the global average the magnetic perturbation magnitude for the case with non-migrating tides in the E- and F-region is around 10 % of the magnetic perturbation for the case with migrating and non-migrating tidal forcing. And for non-migrating tides in the F-region alone the influence decreases to approximately 2.5 % of the full-tide case. These are rough estimates based on this particular solar minimum simulation.

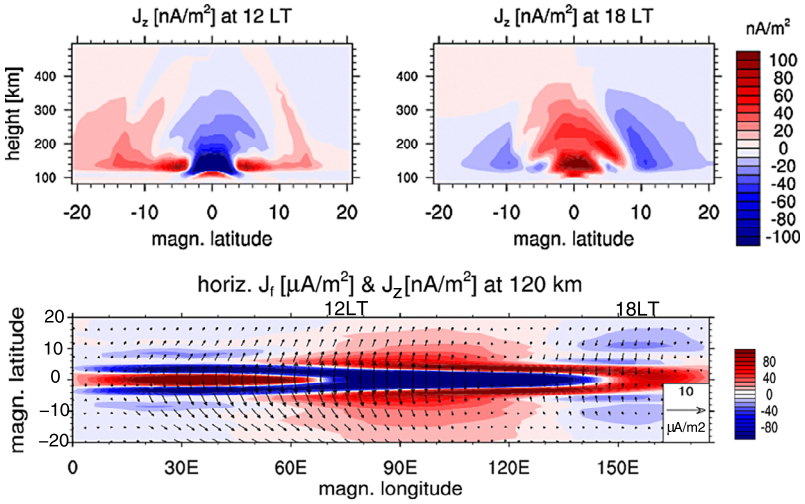

Fig. 9 Top plots: vertical current density J_z component [nA/m^2] at approximately local noon (left, $\phi_m = 75°$ magnetic longitude) and approximately 18 LT (right, $\phi_m = 160°$ magnetic longitude). The bottom panel illustrates the horizontal current density (*arrows*) and the vertical current (*contours*) at 120 km. Conditions are for June at 12 UT, solar medium ($F_{10.7} = 140$ sfu) based on empirical winds and conductivities

In general non-migrating tides have a stronger signature in the ionospheric current than in the magnetic perturbation since the latter is influenced by the changes in the whole ionosphere. This is also reflected in the different longitudinal variations of the current and magnetic perturbations in the case of non-migrating tides in the F-region (Fig. 8 bottom panels). The magnetic perturbation variation at 300 km is largely influenced by an equatorial eastward current flowing in the E-region during the daytime.

These results indicate that when analyzing observed longitudinal variation in magnetic perturbations at equatorial latitudes E- and F-region non-migrating tides have to be considered while at low and midlatitudes the E-region non-migrating tidal contribution dominates (comparing Fig. 8 top and bottom right panels) supporting results from Park and Lühr (2012) based on lunar modulation of the equatorial vertical F-region current. Park et al. (2010) found a wave 4 magnitude in the $\pm 15°$ latitudinally integrated vertical current of around 1 mA/m. Assuming that the current flows between $\pm 15°$ magnetic latitude this corresponds to roughly 0.56 nA/m^2. This cannot be directly compared with the current depicted in Fig. 8 since it includes all non-migrating tides and is not for similar conditions.

3.5 E- and F-Region Wind Driven Current System

To be able to compare with observations E- and F-region winds have to be considered together. Even then the equatorial vertical current can be attributed to the F-region dynamo as identified by Rishbeth (1971a,b). The simulated vertical current density is depicted in Fig. 9 at local noon (left panel) and 18 LT (right panel) for June ($F_{10.7} = 120$ sfu; 12 UT). The wind is specified by the Horizontal Wind Model 93 (Hedin et al. 1996) and the conductivities are calculated based on MSIS and IRI output.

The model can reproduce the general features of the observed current system at LEO altitudes with downward current between $\pm 5°$ magnetic latitude at noon, and upward current at dusk. The closing of the current in the E-region is illustrated in Fig. 9 bottom with a

horizontal slice at 120 km. It indicates strong poleward (equatorward) current right off the magnetic equator at local noon (dusk). Note that the vertical current directions at this altitude generally correspond to those throughout the 120–200 km height range. The meridional current flow (see vectors) away from the equator at this height within $\pm 10^\circ$ of the magnetic equator are in the direction that helps close these vertical currents in the meridional plane. At LEO altitudes vertical current densities derived from Swarm data indicated that the width of the downward noon (upward dusk) current around 470 km is $\pm 2.5^\circ$ ($\pm 5^\circ$) with magnitudes of 3 nA/m^2 (Lühr et al. 2015). In Fig. 9 the current is strongly varying with height and at 400 km has magnitudes similar to the ones observed by Swarm (not visible in Fig. 9 since the magnitude is smaller than the contour level). Differences are expected since the study by Lühr et al. (2015) is based on Swarm measurements between April to November 2014 with solar flux ranging from $F_{10.7} = 120$ sfu to 155 sfu while the simulation is for June conditions with $F_{10.7} = 120$ sfu. The vertical current changes direction between 16.5 and 17 LT which has reasonable agreement with studies from Park and Lühr (2013), Lühr et al. (2015).

Horizontal currents are difficult to deduce from a single satellite. Shore et al. (2013) used crossings of CHAMP and Ørsted to estimate the zonal current density. Based on the 24 crossings they could not find a consistent pattern, and the overall magnitudes were less than 20 nA/m^2. Using the Swarm constellation a more comprehensive picture of the zonal current was developed. In general during the daytime eastward current densities of approximately 20 nA/m^2 were derived while at night westward current prevails with magnitudes around 10 nA/m^2 (Lühr et al. 2016; Tozzi et al. 2015). The simulated zonal current at 400 km peaks at 5 nA/m^2 and even when considering the different geophysical conditions is smaller than the observed one. Further studies will examine the discrepancies between the simulation and the observations.

4 Summary

This article is focused on the effects of the F-region dynamo on the ionospheric current and magnetic perturbations. We briefly summarize the main points. The effects of the F-region dynamo were first pointed out by Rishbeth (1971b) who found that the F-region wind leads to vertical current at the magnetic equator which can close through the E-region during the day and that strong polarization electric fields and plasma drifts are generated, especially at night. Satellites were able to confirm these vertical currents and found approximate magnitudes of 3 nA/m^2 (e.g., Maeda et al. 1982; Olsen 1997; Lühr and Maus 2006; Lühr et al. 2015).

Numerical models can reproduce the general features of the plasma drift and the current system with the westward F-region wind generating an equatorial downward current during the daytime and an upward current at dusk when the F-region wind reverses sign. The current tends to close in the meridional plane close to the equator as described by Rishbeth (1971b). For simulating an accurate local time variation of the vertical current it is crucial to have realistic F-region wind and conductivity variations.

The effects of the F-region dynamo on the ionospheric current and magnetic perturbations are most significant during the daytime when the conductivities are much larger than at nighttime. However during the nighttime the F-region winds are predominately responsible for setting up low and middle latitude electric fields and generating the drift variation.

The F-region dynamo is most effective during solar maximum conditions when the Pedersen conductivity is significantly increased compared to the E-region Hall conductivity (e.g., Crain et al. 1993a). Therefore the magnetic perturbation associated with the F-region

dynamo tends to be larger during solar maximum than minimum conditions, and the relative importance compared to the E-region contributions increases. At middle and low latitude the daytime F-region dynamo can produce comparable and even larger magnetic perturbations at LEO altitude than the E-region dynamo. These low and middle latitude magnetic perturbations are generated by a daytime eastward Hall current in the E-region perpendicular to the upward/poleward polarization electric fields. During solar minimum this effect is less important.

Non-migrating tidal winds in the F-region have been derived from satellite observations (e.g., Häusler and Lühr 2009; Cho and Shepherd 2015; Xiong et al. 2015; Oberheide et al. 2011; Häusler et al. 2010), introducing a regular variation which depends on longitude and local time. Wave number 4 features were found in the in CHAMP vertical F-region current at low latitudes (Park et al. 2010). Numerical simulations indicate that the F-region non-migrating tidal effect on the current and magnetic perturbations is confined to $\pm 10^{\circ}$ magnetic latitude. The current system due to F-region non-migrating tides tends to close in the meridional plane and therefore is not generating significant ground magnetic perturbations. The magnetic perturbation at LEO altitude due to the F-region non-migrating tidal wind is mainly influenced by the setup of a daytime EEJ. Overall the simulation indicates that the E-region non-migrating tides are more effective than F-region non-migrating tides in generating a signal in the current and magnetic perturbations.

Accurately simulating the ionospheric current and magnetic perturbation depends on realistic wind fields and conductivity variations. Observations of neutral winds in the E- and F-region are still sparse and limit our ability to capture realistic ionospheric variations. The F-region dynamo dominates at night the low latitude drift variation and depends significantly on the conductivity distribution. Improved modeling of the nighttime ion density distribution would advance out predictive capabilities.

Acknowledgements This work was supported by NSF grant AGS-1135446. The National Center for Atmospheric Research is sponsored by the National Science Foundation.

References

T.L. Aggson, N.C. Maynard, F.A. Herrero, H.G. Mayr, L.H. Brace, M.C. Liebrecht, Geomagnetic equatorial anomaly in zonal plasma flow. J. Geophys. Res. **92**(A1), 311–315 (1987). doi:10.1029/JA092iA01p00311

S.-I. Akasofu, R. Dewitt, Dynamo action in the ionosphere and motions of the magnetospheric plasma. Planet. Space Sci. **13**(8), 737–744 (1965). doi:10.1016/0032-0633(65)90110-8

P. Alken, S. Maus, A.D. Richmond, A. Maute, The ionospheric gravity and diamagnetic current systems. J. Geophys. Res. **116**(A12), a12316 (2011). doi:10.1029/2011JA017126

P. Alken, A.D. Richmond, A. Maute, Ionospheric gravity and pressure gradient current. Space Sci. Rev. (2016, submitted)

B. Anderson, H. Korth, C. Waters, D. Green, P. Stauning, Statistical birkeland current distributions from magnetic field observations by the Iridium constellation. Ann. Geophys. **26**(3), 671–687 (2008). Copernicus GmbH

D. Anderson, M. Mendillo, Ionospheric conditions affecting the evolution of equatorial plasma depletions. Geophys. Res. Lett. **10**(7), 541–544 (1983)

E.V. Appleton, The anomalous equatorial belt in the F2-layer. J. Atmos. Sol.-Terr. Phys. **5**(1), 348–351 (1954). doi:10.1016/0021-9169(54)90054-9

W.G. Baker, D.F. Martyn, Electric currents in the ionosphere. I. The conductivity. Philos. Trans. R. Soc., Math. Phys. Eng. Sci. **246**(913), 281–294 (1953). doi:10.1098/rsta.1953.0016

D. Bilitza, K. Rawer, L. Bossy, T. Gulyaeva, International reference ionosphere—past, present, and future: I. Electron density. Adv. Space Res. **13**(3), 3–13 (1993)

R.G. Burnside, J.C.G. Walker, R.A. Behnke, C.A. Gonzales, Polarization electric fields in the nighttime F layer at Arecibo. J. Geophys. Res. **88**(A8), 6259–6266 (1983). doi:10.1029/JA088iA08p06259

Y.-M. Cho, G. Shepherd, Resolving daily wave 4 nonmigrating tidal winds at equatorial and midlatitudes with WINDII: DE3 and SE2. J. Geophys. Res. **120**(11), 10,053–10,068 (2015). doi:10.1002/2015JA021903

W.R. Coley, R.A. Heelis, Low-latitude zonal and vertical ion drifts seen by DE 2. J. Geophys. Res. **94**(A6), 6751–6761 (1989). doi:10.1029/JA094iA06p06751

W.R. Coley, R.A. Heelis, N.W. Spencer, Comparison of low-latitude ion and neutral zonal drifts using DE 2 data. J. Geophys. Res. **99**(A1), 341–348 (1994). doi:10.1029/93JA02205

W.R. Coley, R.A. Stoneback, R.A. Heelis, M.R. Hairston, Topside equatorial zonal ion velocities measured by C/NOFS during rising solar activity. Ann. Geophys. **32**(2), 69–75 (2014). doi:10.5194/angeo-32-69-2014

D.J. Crain, R.A. Heelis, G.J. Bailey, Effects of electrical coupling on equatorial ionospheric plasma motions: when is the F-region a dominant driver in the low-latitude dynamo? J. Geophys. Res. **98**(A4), 6033–6037 (1993a). doi:10.1029/92JA02195

D.J. Crain, R.A. Heelis, G.J. Bailey, A.D. Richmond, Low-latitude plasma drifts from a simulation of the global atmospheric dynamo. J. Geophys. Res. **98**(A4), 6039–6046 (1993b). doi:10.1029/92JA02196

R.E. Dickinson, E. Ridley, R. Roble, Thermospheric general circulation with coupled dynamics and composition. J. Atmos. Sci. **41**(2), 205–219 (1984)

V. Doumbia, A. Maute, A.D. Richmond, Simulation of equatorial electrojet magnetic effects with the thermosphere-ionosphere-electrodynamics general circulation model. J. Geophys. Res. **112**(A9), a09309 (2007). doi:10.1029/2007JA012308

J.V. Eccles, Modeling investigation of the evening prereversal enhancement of the zonal electric field in the equatorial ionosphere. J. Geophys. Res. **103**(A11), 26,709–26,719 (1998a). doi:10.1029/98JA02656

J.V. Eccles, A simple model of low-latitude electric fields. J. Geophys. Res. **103**(A11), 26,699–26,708 (1998b). doi:10.1029/98JA02657

J.V. Eccles, The effect of gravity and pressure in the electrodynamics of the low-latitude ionosphere. J. Geophys. Res. **109**(A5), A05304 (2004). doi:10.1029/2003JA010023

J.V. Eccles, N. Maynard, G. Wilson, Study of the evening plasma drift vortex in the low-latitude ionosphere using San Marco electric field measurements. J. Geophys. Res. **104**(A12), 28,133–28,143 (1999). doi:10.1029/1999JA900373

J.V. Eccles, J.P.St. Maurice, R.W. Schunk, Mechanisms underlying the prereversal enhancement of the vertical plasma drift in the low-latitude ionosphere. J. Geophys. Res. **120**(6), 4950–4970 (2015). doi:10.1002/2014JA020664

S.L. England, T.J. Immel, J.D. Huba, M.E. Hagan, A. Maute, R. DeMajistre, Modeling of multiple effects of atmospheric tides on the ionosphere: an examination of possible coupling mechanisms responsible for the longitudinal structure of the equatorial ionosphere. J. Geophys. Res. **115**(A5), A05308 (2010). doi:10.1029/2009JA014894

W. Evonosky, A.D. Richmond, T.-W. Fang, A. Maute, Ion-neutral coupling effects on low-latitude thermospheric evening winds. J. Geophys. Res. Space Phys. **121**, 4638–4646 (2016). doi:10.1002/2016JA022382

D.T. Farley, A theory of electrostatic fields in a horizontally stratified ionosphere subject to a vertical magnetic field. J. Geophys. Res. **64**(9), 1225–1233 (1959). doi:10.1029/JZ064i009p01225

D.T. Farley, E. Bonelli, B.G. Fejer, M.F. Larsen, The prereversal enhancement of the zonal electric field in the equatorial ionosphere. J. Geophys. Res. **91**(A12), 13,723–13,728 (1986). doi:10.1029/JA091iA12p13723

B. Fejer, D. Farley, R. Woodman, C. Calderon, Dependence of equatorial F region vertical drifts on season and solar cycle. J. Geophys. Res. **84**(A10), 5792–5796 (1979). doi:10.1029/JA084iA10p05792

B.G. Fejer, The equatorial ionospheric electric fields. A review. J. Atmos. Sol.-Terr. Phys. **43**(5–6), 377–386 (1981). doi:10.1016/0021-9169(81)90101-X

B.G. Fejer, Low latitude ionospheric electrodynamics. Space Sci. Rev. **158**, 145–166 (2011). doi:10.1007/s11214-010-9690-7

B.G. Fejer, E. Kudeki, D.T. Farley, Equatorial F region zonal plasma drifts. J. Geophys. Res. **90**(A12), 12,249–12,255 (1985). doi:10.1029/JA090iA12p12249

B.G. Fejer, E.R. de Paula, S.A. González, R.F. Woodman, Average vertical and zonal F region plasma drifts over Jicamarca. J. Geophys. Res. **96**(A8), 13,901–13,906 (1991). doi:10.1029/91JA01171

B.G. Fejer, J.R. Souza, A.S. Santos, A.E. Costa Pereira, Climatology of F region zonal plasma drifts over Jicamarca. J. Geophys. Res. **110**(A12), a12310 (2005). doi:10.1029/2005JA011324

B.G. Fejer, B.D. Tracy, R.F. Pfaff, Equatorial zonal plasma drifts measured by the C/NOFS satellite during the 2008–2011 solar minimum. J. Geophys. Res. **118**(6), 3891–3897 (2013). doi:10.1002/jgra.50382

B.G. Fejer, D. Hui, J.L. Chau, E. Kudeki, Altitudinal dependence of evening equatorial F region vertical plasma drifts. J. Geophys. Res. **119**(7), 5877–5890 (2014). doi:10.1002/2014JA019949

C.G. Fesen, G. Crowley, R.G. Roble, A.D. Richmond, B.G. Fejer, Simulation of the pre-reversal enhancement in the low latitude vertical ion drifts. Geophys. Res. Lett. **27**(13), 1851–1854 (2000). doi:10.1029/2000GL000061

J.M. Forbes, The equatorial electrojet. Rev. Geophys. **19**(3), 469–504 (1981)

J. Geisler, A numerical study of the wind system in the middle thermosphere. J. Atmos. Sol.-Terr. Phys. **29**(12), 1469–1482 (1967). doi:10.1016/0021-9169(67)90100-6

D.L. Green, C.L. Waters, B.J. Anderson, H. Korth, Seasonal and interplanetary magnetic field dependence of the field-aligned currents for both northern and southern hemispheres. Ann. Geophys. **27**(4), 1701–1715 (2009). doi:10.5194/angeo-27-1701-2009

G. Haerendel, J.V. Eccles, S. Çakir, Theory for modeling the equatorial evening ionosphere and the origin of the shear in the horizontal plasma flow. J. Geophys. Res. **97**(A2), 1209–1223 (1992). doi:10.1029/91JA02226

M. Hagan, J. Forbes, Migrating and nonmigrating semidiurnal tides in the upper atmosphere excited by tropospheric latent heat release. J. Geophys. Res. **108**(1062), 10–1029 (2003)

M.E. Hagan, J.M. Forbes, Migrating and nonmigrating diurnal tides in the middle and upper atmosphere excited by tropospheric latent heat release. J. Geophys. Res., Atmos. **107**(D24), ACL 6-1–ACL 6-15 (2002). doi:10.1029/2001JD001236

M.E. Hagan, A. Maute, R.G. Roble, Tropospheric tidal effects on the middle and upper atmosphere. J. Geophys. Res. **114**(A1), A01302 (2009). doi:10.1029/2008JA013637

K. Häusler, H. Lühr, Nonmigrating tidal signals in the upper thermospheric zonal wind at equatorial latitudes as observed by CHAMP. Ann. Geophys. **27**(7), 2643–2652 (2009)

K. Häusler, H. Lühr, M.E. Hagan, A. Maute, R.G. Roble, Comparison of CHAMP and TIME-GCM nonmigrating tidal signals in the thermospheric zonal wind. J. Geophys. Res., Atmos. **115**(D1), D00I08 (2010). doi:10.1029/2009JD012394

A. Hedin, Extension of the MSIS thermospheric model into the middle and lower atmosphere. J. Geophys. Res. **96**(A2), 1159–1172 (1991)

A.E. Hedin et al., Empirical wind model for the upper, middle and lower atmosphere. J. Atmos. Sol.-Terr. Phys. **58**(13), 1421–1447 (1996)

R. Heelis, P. Kendall, R. Moffett, D. Windle, H. Rishbeth, Electrical coupling of the E- and F-regions and its effect on F-region drifts and winds. Planet. Space Sci. **22**(5), 743–756 (1974). doi:10.1016/0032-0633(74)90144-5

R.A. Heelis, Electrodynamics in the low and middle latitude ionosphere: a tutorial. J. Atmos. Sol.-Terr. Phys. **66**, 825–838 (2004). doi:10.1016/j.jastp.2004.01.034

R.A. Heelis, J.K. Lowell, R.W. Spiro, A model of the high-latitude ionospheric convection pattern. J. Geophys. Res. **87**(A8), 6339–6345 (1982). doi:10.1029/JA087iA08p06339

R.A. Heelis, G. Crowley, F. Rodrigues, A. Reynolds, R. Wilder, I. Azeem, A. Maute, The role of zonal winds in the production of a pre-reversal enhancement in the vertical ion drift in the low latitude ionosphere. J. Geophys. Res. **117**(A8), a08308 (2012). doi:10.1029/2012JA017547

M. Hirono, A theory of diurnal magnetic variations in equatorial regions and conductivity of the ionospheric E region. J. Geomagn. Geoelectr. **4**, 7–21 (1952)

J.D. Huba, G. Joyce, J. Krall, C.L. Siefring, P. Bernhardt, Self-consistent modeling of equatorial dawn density depletions with SAMI3. Geophys. Res. Lett. **37**(3), L03104 (2010a). doi:10.1029/2009GL041492

J.D. Huba, G. Joyce, J. Krall, C.L. Siefring, P.A. Bernhardt, Correction to "Self-consistent modeling of equatorial dawn density depletions with SAMI3". Geophys. Res. Lett. **37**(20), L20104 (2010b). doi:10.1029/2010GL045004

T. Iijima, Field-aligned currents in geospace: substance and significance, in *Magnetospheric Current Systems*, ed. by S.-I. Ohtani, R. Fujii, M. Hesse, R.L. Lysak (Am. Geophys. Union, Washington, 2000). doi:10.1029/GM118p0107

T.J. Immel, E. Sagawa, S.L. England, S.B. Henderson, M.E. Hagan, S.B. Mende, H.U. Frey, C.M. Swenson, L.J. Paxton, Control of equatorial ionospheric morphology by atmospheric tides. Geophys. Res. Lett. **33**(15), L15108 (2006). doi:10.1029/2006GL026161

H. Jin, Y. Miyoshi, H. Fujiwara, H. Shinagawa, K. Terada, N. Terada, M. Ishii, Y. Otsuka, A. Saito, Vertical connection from the tropospheric activities to the ionospheric longitudinal structure simulated by a new Earth's whole atmosphere-ionosphere coupled model. J. Geophys. Res. **116**(A1), a01316 (2011). doi:10.1029/2010JA015925

M. Jones, J.M. Forbes, M.E. Hagan, A. Maute, Non-migrating tides in the ionosphere-thermosphere: in situ versus tropospheric sources. J. Geophys. Res. **118**(5), 2438–2451 (2013). doi:10.1002/jgra.50257

M.V. Klimenko, V.V. Klimenko, V.V. Bryukhanov, Numerical simulation of the electric field and zonal current in the Earth's ionosphere: the dynamo field and equatorial electrojet. Geomagn. Aeron. **46**, 457–466 (2006). doi:10.1134/S0016793206040074

E. Kudeki, S. Bhattacharyya, Postsunset vortex in equatorial F-region plasma drifts and implications for bottomside spread-F. J. Geophys. Res. **104**(A12), 28,163–28,170 (1999). doi:10.1029/1998JA900111
E. Kudeki, B.G. Fejer, D.T. Farley, H.M. Ierkic, Interferometer studies of equatorial F region irregularities and drifts. Geophys. Res. Lett. **8**(4), 377–380 (1981). doi:10.1029/GL008i004p00377
W.K. Lee, H. Kil, Y.-S. Kwak, L.J. Paxton, Morphology of the postsunset vortex in the equatorial ionospheric plasma drift. Geophys. Res. Lett. **42**(1), 9–14 (2015). doi:10.1002/2014GL062019
R. Lindzen, Atmospheric tides. Annu. Rev. Earth Planet. Sci. **7**, 199–225 (1979)
H. Lühr, S. Maus, Direct observation of the F region dynamo currents and the spatial structure of the EEJ by CHAMP. Geophys. Res. Lett. **33**(24), l24102 (2006). doi:10.1029/2006GL028374
H. Lühr, M. Rother, S. Maus, W. Mai, D. Cooke, The diamagnetic effect of the equatorial appleton anomaly: its characteristics and impact on geomagnetic field modeling. Geophys. Res. Lett. **30**(17), 1906 (2003). doi:10.1029/2003GL017407
H. Lühr, G. Kervalishvili, I. Michaelis, J. Rauberg, P. Ritter, J. Park, J.M.G. Merayo, P. Brauer, The inter-hemispheric and F region dynamo currents revisited with the Swarm constellation. Geophys. Res. Lett. **42**(9), 3069–3075 (2015). doi:10.1002/2015GL063662
H. Lühr, G. Kervalishvili, J. Rauberg, C. Stolle, Zonal currents in the F region deduced from Swarm constellation measurements. J. Geophys. Res. (2016). doi:10.1002/2015JA022051
M.K. Madhav Haridas, G. Manju, T.K. Pant, On the solar activity variations of nocturnal F region vertical drifts covering two solar cycles in the Indian longitude sector. J. Geophys. Res. **120**(2), 1445–1451 (2015). doi:10.1002/2014JA020561
H. Maeda, T. Iyemori, T. Araki, T. Kamei, New evidence of a meridional current system in the equatorial ionosphere. Geophys. Res. Lett. **9**(4), 337–340 (1982). doi:10.1029/GL009i004p00337
H. Maeda, T. Kamei, T. Iyemori, T. Araki, Geomagnetic perturbations at low latitudes observed by Magsat. J. Geophys. Res., Solid Earth **90**(B3), 2481–2486 (1985). doi:10.1029/JB090iB03p02481
T.J. Mathew, S.P. Nayar, Vertical shear at the equatorial F-region ionosphere during post-sunset hours. Adv. Space Res. **49**(8), 1277–1281 (2012). doi:10.1016/j.asr.2012.01.011
N. Matuura, Electric fields deduced from the thermospheric model. J. Geophys. Res. **79**(31), 4679–4689 (1974). doi:10.1029/JA079i031p04679
S. Maus, H. Lühr, A gravity-driven electric current in the Earth's ionosphere identified in CHAMP satellite magnetic measurements. Geophys. Res. Lett. **33**(2), L02812 (2006). doi:10.1029/2005GL024436
A. Maute, A.D. Richmond, R.G. Roble, Sources of low-latitude ionospheric ExB drifts and their variability. J. Geophys. Res. **117**(A6), A06312 (2012). doi:10.1029/2011JA017502
G.H. Millward, I.C.F. Müller-Wodarg, A.D. Aylward, T.J. Fuller-Rowell, A.D. Richmond, R.J. Moffett, An investigation into the influence of tidal forcing on F region equatorial vertical ion drift using a global ionosphere-thermosphere model with coupled electrodynamics. J. Geophys. Res. **106**(A11), 24,733–24,744 (2001). doi:10.1029/2000JA000342
A. Namgaladze, Y. Korenkov, V. Klimenko, F.B.I.V. Karpov, V. Surotkin, T. Glushchenko, N. Naumova, Global model of the thermosphere-ionosphere-protonosphere system. Pure Appl. Geophys. **127**, 219–254 (1988)
J. Oberheide, J.M. Forbes, X. Zhang, S.L. Bruinsma, Wave-driven variability in the ionosphere-thermosphere-mesosphere system from TIMED observations: what contributes to the "wave 4"? J. Geophys. Res. **116**(A1), A01306 (2011). doi:10.1029/2010JA015911
S. Ohtani, G. Ueno, T. Higuchi, Comparison of large-scale field-aligned currents under sunlit and dark ionospheric conditions. J. Geophys. Res. **110**(A9), A09230 (2005). doi:10.1029/2005JA011057
N. Olsen, Ionospheric F region currents at middle and low latitudes estimated from magsat data. J. Geophys. Res. **102**(A3), 4563–4576 (1997). doi:10.1029/96JA02949
E.E. Pacheco, R.A. Heelis, S.-Y. Su, Quiet time meridional (vertical) ion drifts at low and middle latitudes observed by ROCSAT-1. J. Geophys. Res. **115**(A9), a09308 (2010). doi:10.1029/2009JA015108
D. Pancheva, Y. Miyoshi, P. Mukhtarov, H. Jin, H. Shinagawa, H. Fujiwara, Global response of the ionosphere to atmospheric tides forced from below: comparison between COSMIC measurements and simulations by atmosphere-ionosphere coupled model GAIA. J. Geophys. Res. **117**(A7), A07319 (2012). doi:10.1029/2011JA017452
J. Park, H. Lühr, Effects of sudden stratospheric warming (SSW) on the lunitidal modulation of the F-region dynamo. J. Geophys. Res. **117**(A9), A09320 (2012). doi:10.1029/2012JA018035
J. Park, H. Lühr, Relation of zonal plasma drift and wind in the equatorial F region as derived from CHAMP observations. Ann. Geophys. **31**(6), 1035–1044 (2013)
J. Park, H. Lühr, K.W. Min, Characteristics of F-region dynamo currents deduced from champ magnetic field measurements. J. Geophys. Res. **115**(A10), a10302 (2010). doi:10.1029/2010JA015604
J. Park, H. Lühr, K.W. Min, Climatology of the inter-hemispheric field-aligned current system in the equatorial ionosphere as observed by CHAMP. Ann. Geophys. **29**, 573–582 (2011). doi:10.5194/angeo-29-573-2011

T.A. Potemra, Field-aligned (Birkeland) currents. Space Sci. Rev. **42**(3–4), 295–311 (1985)
L. Qian et al., The NCAR TIE-GCM: a community model of the coupled thermosphere/ionosphere system, in *Modeling the Ionosphere-Thermosphere System*. Geophys. Monogr. Ser., vol. 201 (2014), pp. 73–83
R. Rastogi, The equatorial electrojet: magnetic and ionospheric effects. Geomagnetism **3**, 461–525 (1989)
Z. Ren, W. Wan, L. Liu, GCITEM-IGGCAS: a new global coupled ionosphere-thermosphere-electrodynamics model. J. Atmos. Sol.-Terr. Phys. **71**(17), 2064–2076 (2009)
A. Richmond, Ionospheric wind dynamo theory: a review. J. Geomagn. Geoelectr. **31**(3), 287–310 (1979)
A. Richmond, A. Maute, Ionospheric electrodynamics modeling, in *Modeling the Ionosphere-Thermosphere System* (2014), pp. 57–71. doi:10.1002/9781118704417.ch6
A.D. Richmond, Ionospheric electrodynamics using magnetic apex coordinates. J. Geomagn. Geoelectr. **47**(2), 191–212 (1995)
A.D. Richmond, T.-W. Fang, Electrodynamics of the equatorial evening ionosphere: 2. Conductivity influences on convection, current, and electrodynamic energy flow. J. Geophys. Res. (2015). doi:10.1002/2014JA020935
A.D. Richmond, E.C. Ridley, R.G. Roble, A thermosphere/ionosphere general circulation model with coupled electrodynamics. Geophys. Res. Lett. **19**(6), 601–604 (1992). doi:10.1029/92GL00401
A.D. Richmond, T.-W. Fang, A. Maute, Electrodynamics of the equatorial evening ionosphere: 1. Importance of winds in different regions. J. Geophys. Res. (2015). doi:10.1002/2014JA020934
H. Rishbeth, The F-layer dynamo. Planet. Space Sci. **19**(2), 263–267 (1971a)
H. Rishbeth, Polarization fields produced by winds in the equatorial F-region. Planet. Space Sci. **19**(3), 357–369 (1971b). doi:10.1016/0032-0633(71)90098-5
H. Rishbeth, The F-region dynamo. J. Atmos. Sol.-Terr. Phys. **43**(56), 387–392 (1981). Equatorial Aeronomy—I. doi:10.1016/0021-9169(81)90102-1
H. Rishbeth, The ionospheric E-layer and F-layer dynamos: a tutorial review. J. Atmos. Sol.-Terr. Phys. **59**(15), 1873–1880 (1997). doi:10.1016/S1364-6826(97)00005-9
R. Roble, E. Ridley, A. Richmond, A coupled thermosphere/ionosphere general circulation model. Geophys. Res. Lett. **15**, 1325–1328 (1988)
R.G. Roble, Modeling the dynamics of the coupled thermosphere and ionosphere, in *Solar-Terrestrial Energy Program*, ed. by D.N. Baker, V.O. Papitashvili, M.J. Teague (1994), p. 765
F.S. Rodrigues, G. Crowley, R.A. Heelis, A. Maute, A. Reynolds, On TIE-GCM simulation of the evening equatorial plasma vortex. J. Geophys. Res. **117**(A5), A05307 (2012). doi:10.1029/2011JA017369
L. Scherliess, B.G. Fejer, Radar and satellite global equatorial F-region vertical drift model. J. Geophys. Res. **104**(A4), 6829–6842 (1999)
R.M. Shore, K.A. Whaler, S. Macmillan, C. Beggan, N. Olsen, T. Spain, A. Aruliah, Ionospheric midlatitude electric current density inferred from multiple magnetic satellites. J. Geophys. Res. **118**(9), 5813–5829 (2013). doi:10.1002/jgra.50491
B. Stewart, Terrestrial magnetism. Encycl. Britannica **16**(181), 31 (1882)
R. Stoneback, R. Heelis, A. Burrell, W. Coley, B.G. Fejer, E. Pacheco, Observations of quiet time vertical ion drift in the equatorial ionosphere during the solar minimum period of 2009. J. Geophys. Res. **116**(A12), A12327 (2011)
M. Takeda, H. Maeda, F-region dynamo in the evening—interpretation of equatorial δd anomaly found by magsat. J. Atmos. Sol.-Terr. Phys. **45**(6), 401–408 (1983)
E. Thébault et al., International geomagnetic reference field: the 12th generation. Earth Planets Space **67**(1), 1–19 (2015)
R. Tozzi, M. Pezzopane, P. De Michelis, M. Piersanti, Applying a curl-B technique to Swarm vector data to estimate nighttime F region current intensities. Geophys. Res. Lett. **42**(15), 6162–6169 (2015)
R. Tsunoda, R. Livingston, C. Rino, Evidence of a velocity shear in bulk plasma motion associated with the post-sunset rise of the equatorial F-layer. Geophys. Res. Lett. **8**(7), 807–810 (1981)
H. Volland, Coupling between the neutral tidal wind and the ionospheric dynamo current. J. Geophys. Res. **81**(10), 1621–1628 (1976a)
H. Volland, The atmospheric dynamo. J. Atmos. Sol.-Terr. Phys. **38**(8), 869–877 (1976b)
D. Weimer, Maps of ionospheric field-aligned currents as a function of the interplanetary magnetic field derived from Dynamics Explorer 2 data. J. Geophys. Res. **106**(A7), 12,889–12,902 (2001)
R.F. Woodman, Vertical drift velocities and east-west electric fields at the magnetic equator. J. Geophys. Res. **75**(31), 6249–6259 (1970)
C. Xiong, H. Lühr, C. Stolle, Seasonal and latitudinal variations of the electron density nonmigrating tidal spectrum in the topside ionospheric F region as resolved from CHAMP observations. J. Geophys. Res. **119**(12), 10,416–10,425 (2014). doi:10.1002/2014JA020354
C. Xiong, Y. Zhou, H. Lühr, S. Ma, Tidal signatures of the thermospheric mass density and zonal wind at midlatitude: CHAMP and GRACE observations. Ann. Geophys. **33**, 185–196 (2015)

K. Yamashita, S. Miyahara, Y. Miyoshi, K. Kawano, J. Ninomiya, Seasonal variation of non-migrating semidiurnal tide in the polar MLT region in a general circulation model. J. Atmos. Sol.-Terr. Phys. **64**(811), 1083–1094 (2002). doi:10.1016/S1364-6826(02)00059-7

Y. Yamazaki, A. Maute, Sq and EEJ—a review on the daily variation of the geomagnetic field caused by ionopsheric dynamo currents. Space Sci. Rev. (2016, submitted)